JCTC Journal of Chemical Theory and Computation

Absorption Spectra of the Potential Photodynamic Therapy Photosensitizers Texaphyrins Complexes: A Theoretical Analysis†

Angelo Domenico Quartarolo,‡ Nino Russo,*,‡ Emilia Sicilia,‡ and Francesco Lelj§

Dipartimento di Chimica and Centro di Calcolo ad Alte Prestazioni per Elaborazioni Parallele e Distribuite-Centro d'Eccellenza MURST, Università della Calabria, I-87030 Arcavacata di Rende, Italy, and Dipartimento di Chimica, Università degli Studi della Basilicata, Via Nazario Sauro, 85, 85100 Potenza

Received December 22, 2006

Abstract: A systematic study of a class of divalent transition-metal texaphyrin complexes (M-Tex$^+$, M = Mn, Fe, Co, Ni, Cu, Zn), recently proposed as active photosensitizers in photodynamic therapy (PDT), was undertaken for the ground and excited electronic states. Geometry optimizations were performed by using the PBE0 exchange-correlation functional coupled with the 6-31G(d) basis set, while electronic excitations energies were evaluated by means of time-dependent density functional response theory (TD-DFT) at the PBE0/6-31+G(d) // PBE0/6-31G(d) level of theory. Solvent effects on excitation energies were taken into account in two ways: by considering solvent molecules explicitly coordinated to the metal center and as bulk effects, within the conductor-like polarizable continuum model (C-PCM). The influence of the metal cation on the so-called Q-band, localized in the near-red visible region of the spectrum, was carefully examined since it plays a basic role in the drug design of new photodynamic therapy photosensitizers. The differences between experimental and computed excitation energies were found to be within 0.3 eV.

1. Introduction

Texaphyrins are a class of expanded porphyrin macrocycles formed by three tripyrrolyldimethene units connected to a phenylenediamine through two imine-type linkages (see Chart 1).[1−3] The main structural feature of texaphyrins is the increased cavity size, about 20% larger than porphyrins, that allows a better fit of the nearly coplanar nitrogen donors, to the metal cation. Metallotexaphyrins (M-Tex) for nearly the full series of lanthanide(III),[4,5] Cd(II),[1,6] Y(III) and In-(III),[7] and for Mn(II) to Zn(II)[8,9] as well as a metal free aromatic form[10] were synthesized during the past few years. The synthesis was carried out by treating the "sp^2-texaphyrin", a nonaromatic form, with metal salt and air, through an oxidation-metalation reaction mechanism. Gadolinium-(III)-Tex^{2+} and lutetium(III)-Tex^{2+}, in a water soluble form, are in late-stage clinical trials for application as an adjuvant in X-ray radiation therapy and photodynamic therapy (PDT), respectively.[11,12]

Photodynamic therapy is a noninvasive medical technique for the treatment of different types of diseases in oncology and ophtalmology.[13−15] The basic principle is the combination of a photosensitizing drug capable of absorbing within the body's therapeutic window (620−850 nm), a light source (e.g., laser) of appropriate wavelength and molecular oxygen. The photosensitizer, which shows preferably high accumulation in cancer cells and low dark toxicity, is injected into human body tissue and then irradiated by visible light. After irradiation the light-activated molecule undergoes different reactions, and it can decay from singlet to triplet excited state, through a radiationless transition (intersystem spin crossing). The rate of the latter step is enhanced by the presence in the

† Dedicated to Professor Dennis R. Salahub on the occasion of his 60th birthday.

* Corresponding author: e-mail: nrusso@unical.it.

‡ Università della Calabria.

§ Università degli Studi della Basilicata.

10.1021/ct600376h CCC: $37.00
Published on Web 04/03/2007

Chart 1

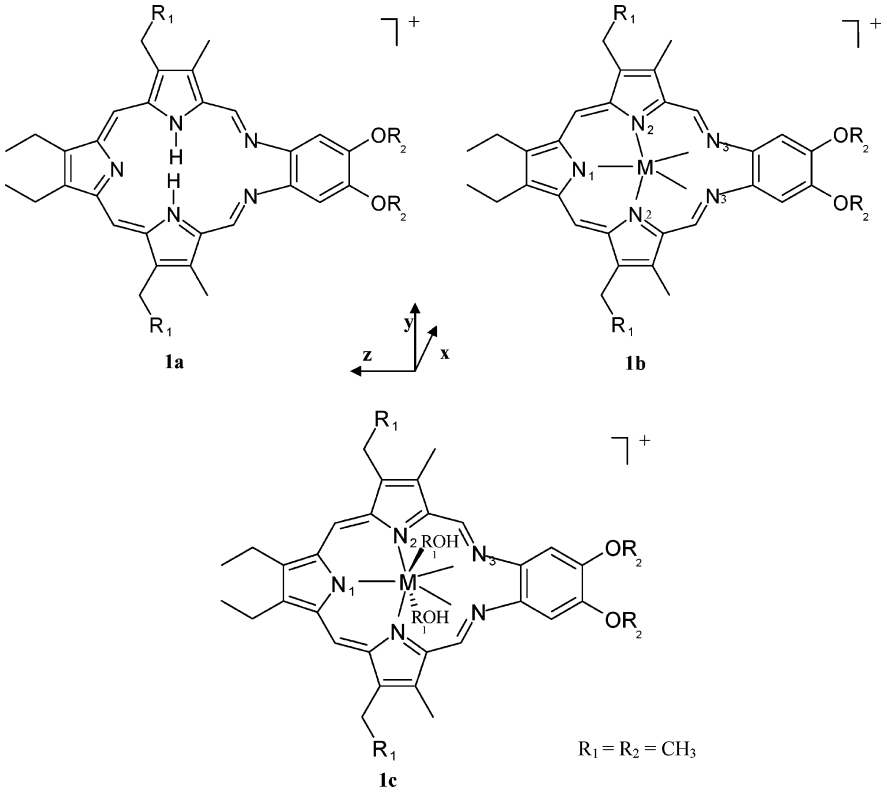

molecule of an atom with a high atomic number (heavy atom effect). The key cytotoxic agent is represented by singlet molecular oxygen $^1O_2$ ($^1\Delta_g$) generated by an energy transfer reaction from the photosensitizer triplet state to the ground state of molecular oxygen $^3O_2$ ($^3\Sigma_g$).[16,17] Triplet state energy should match, for a good efficiency, the first excitation energy of molecular oxygen, that is 0.98 eV (1300 nm). The interest in using metallotexaphyrins in PDT is due to the their spectral absorbance features. In fact, they exhibit Q-type electronic transitions between 650 and 810 nm and are thus red-shifted by more than 100 nm with respect to porphyrins. This property is related to the increased number of π electrons (22 π-electron system) that causes a greater electron delocalization on the aromatic ring. It is desirable in PDT to have Q-bands in the near-red region of the spectra, since light transmittance into human body changes exponentially with the increasing wavelength of the incident radiation. At present, in literature exist few theoretical works regarding metallotexaphyrins. To our knowledge, a B3LYP density functional study using relativistic ab initio pseudopotentials, was carried out by Cao and Dolg[18] for lanthanide(III) texaphyrins [Ln-Tex(3+), Ln = La, Gd, Lu] and more recently for actinide(III) motexafins [An-Tex(3+), An = Ac, Cm, Lr] by Cao et al.[19] Moreover, a theoretical study for the interpretation of the magnetic circular dichroism spectra (MCD) of texaphyrins was performed by Waluk and Michl.[20] The present work deals with a density functional investigation of electronic properties of first-row transition-metal complexes of texaphyrin in organic soluble form (see Chart 1) as well as the evaluation of the electronic excitation energies by means of time-dependent density functional theory (TD-DFT).[21] Our aim is to give new insights from theory in interpreting spectroscopic properties of metallotexaphyrins and to contribute to better characterize this novel class of photosensitizers potentially useful in PDT. To account for the interaction with the local environment solvent effects were included both explicitly by considering two methanol solvent molecules directly bound to the metal center and implicitly by using a continuum solvation model.

2. Computational Details

All calculations were carried out at the density functional level of theory with the GAUSSIAN03 program package.[22] The hybrid functional approach PBE0[23,24] was employed for geometry optimization, vibrational frequency analysis, and electronic excitation energy evaluation. The PBE0 exchange-correlation functional is based on the generalized gradient functional of Perdew-Burke-Ernzerhof (PBE)[25] with an a priori fixed amount of 25% of Hartree−Fock exchange energy. Restricted formalism was applied for closed shell systems (free base texaphyrin and zinc complex) and an unrestricted one for open shell systems. In the latter case spin contamination, monitored by the expectation value of $\hat{S}^2$, was found to be negligible. All molecular structures were fully optimized imposing a C_2 symmetry axis, joining the metal center with the pyrrolic nitrogen atom N_1. For the geometry optimization, a split valence plus polarization basis set 6-31G(d)[26,27] for H, C, N, and O atoms and a double-ζ quality LANL basis and corresponding pseudopotential for metal atoms (Mn, Fe, Ni, Co, Cu, and Zn) were employed.[28,29] Vibrational frequency analysis was used to confirm the character of minima of optimized structures. Electronic excitation energies and oscillator strengths were computed within the adiabatic approximation of time-dependent density functional theory (TD-DFT)[30] as implemented in Gaussian03. The 6-31+G(d) basis set, which adds

a diffuse function to the 6-31G(d) one for all atoms except hydrogen, was used along with the same pseudopotentials and the corresponding valence basis sets for the metal centers. The influence of scalar relativistic effects of first-row transition metals on excitation energies was evaluated by using the Zn-Tex$^+$ complex as a test molecule. For this purpose the Stuttgart relativistic small- and large-core pseudopotentials ECP28SDF and ECP10MWB[31,32] were used for the zinc atom. In order to characterize the electronic spectra of the examined complexes, the same level of theory used in previous works, which demonstrated as the influence on optical transitions of the basis set choice is minimal and the hybrid functional PBE0 gives usually an accuracy, comparable to refined post-Hartree−Fock approaches at a lower computational cost, of about 0.3 eV for the transition energies.[33−36] Bulk solvent effects (methanol, $\epsilon = 32.6$) were taken into account within the conductor-like polarizable continuum model (C-PCM).[37−39] Single-point calculations on the optimized geometries were carried out by the nonequilibrium implementation of C-PCM.[40−43] The electronic spectra were simulated by means of the SWizard program package.[44] Here the absorption profile is calculated as a sum of Gaussian functions using the formula

$$\epsilon(\omega) = 2.174 * 10^8 \sum_I \frac{f_I}{\Delta_{1/2}} \exp\left(-2.773 \frac{(\omega - \omega_I)^2}{\Delta_{1/2}^2}\right)$$

where ϵ is the molar absorbance in units of mol^{-1} cm^{-1} L, the index sum runs over the number of computed excitation energies ω_I (expressed in cm^{-1}) with corresponding oscillator strengths $\times c4_I$, and $\Delta_{1/2}$ is the half-weight bandwidth assumed constant and equal to 3000 cm^{-1}.

3. Results and Discussion

3.1. Ground-State Spin Multiplicity. Our first task was to determine the ground and lowest excited electronic states for M-Tex$^+$ complexes, with and without methanol molecules coordinated to the metal center. As pointed out above, an efficient PDT drug should activate molecular oxygen ($^3O_2$) through an energy transfer, so a preliminary condition to be satisfied is that the electronic gap between ground and first excited states must be greater than or equal to 0.98 eV. For metalloporphyrins-like systems the electronic ground state is influenced by several factors like the ligand size and geometry. For each complex we have considered different spin multiplicities on the basis of the electronic configuration of the divalent metal cation (e.g., ^{6}A, ^{4}A, and ^{2}A electronic states for Mn (d^5) complex). The total and relative energies of the two most stable electronic states of each complex are reported in Table 1. As it can be noted, the electronic ground state for every complex, both isolated and coordinated with two solvent molecules, corresponds to a high-spin multiplicity state. For the Mn-Tex$^+$ complex doublet, quartet, and sextet states were considered. In this case the ground state for the isolated system was found to be a sextet state, whereas the doublet and quartet states lie 4.01 and 4.38 eV higher in energy than the ground state, respectively. On the other hand, for Mn-Tex(CH$_3$OH)$_2^+$ we found for the first excited state an opposite situation: the ^{4}A electronic state is lower in energy than the ^{2}A state (1.68 vs 2.74 eV) with respect to the ^{6}A ground state. For the remaining M-Tex$^+$ bare systems, the lowest state lies in the range between 1.14 eV (Cu-Tex) and 1.32 eV (Zn-Tex). For the explicitly solvated systems the electronic gap is lower and ranges from 0.84 eV (Co-Tex(CH$_3$OH)$_2^+$) to 1.39 eV (Ni-Tex(CH$_3$OH)$_2^+$). Overall, for the isolated systems all M-Tex$^+$ fulfill the ground-excited energetic gap condition (i.e., > 0.98 eV). For systems coordinating two solvent molecules this condition holds for Mn-, Fe-, Ni-, Cu-, and Zn-Tex complexes. These results are in agreement with the experimental measurements of the magnetic moments for each paramagnetic complex,[9] which gives rise to a high-spin configuration state as confirmed by applying the so-called 'spin-only formula'. The only exception is represented by the Fe-Tex$^+$ complex that exists as a dimer, with two Fe(III) atoms bridged by an oxygen (in a formally trivalent oxidation state).

Table 1. Total (hartrees) and Relative Energies (eV) for All Complexes for Bare Systems and with Two Methanol Molecules Coordinated to the Metal Atom

molecule	molecular symmetry	electronic state	total energy (hartrees)	ΔE (eV)
		Isolated Systems		
Mn-Tex$^+$	C_2	^{2}A	−1844.3437	4.01
Mn-Tex$^+$	C_2	^{4}A	−1844.3302	4.38
Mn-Tex$^+$	C_2	^{6}A	−1844.4912	0.00
Fe-Tex$^+$	C_2	^{3}A	−1863.9198	1.16
Fe-Tex$^+$	C_2	^{5}A	−1863.9626	0.00
Co-Tex$^+$	C_2	^{2}A	−1885.5405	0.99
Co-Tex$^+$	C_2	^{4}A	−1885.5770	0.00
Ni-Tex$^+$	C_2	^{1}A	−1909.7602	1.56
Ni-Tex$^+$	C_2	^{3}A	−1909.8184	0.00
Cu-Tex$^+$	C_2	^{4}A	−1936.5941	1.14
Cu-Tex$^+$	C_2	^{2}A	−1936.6022	0.00
Zn-Tex$^+$	C_2	^{3}A	−1805.9484	1.32
Zn-Tex$^+$	C_2	^{1}A	−1805.9970	0.00
		Complexes Coordinating Two Methanol Molecules		
Mn-Tex(MeOH)$_2^+$	C_2	^{2}A	−2075.6041	2.74
Mn-Tex(MeOH)$_2^+$	C_2	^{4}A	−2075.6432	1.68
Mn-Tex(MeOH)$_2^+$	C_2	^{6}A	−2075.7049	0.00
Fe-Tex(MeOH)$_2^+$	C_2	^{3}A	−2095.1434	0.99
Fe-Tex(MeOH)$_2^+$	C_2	^{5}A	−2095.1797	0.00
Co-Tex(MeOH)$_2^+$	C_2	^{2}A	−2116.7665	0.84
Co-Tex(MeOH)$_2^+$	C_2	^{4}A	−2116.7974	0.00
Ni-Tex(MeOH)$_2^+$	C_2	^{1}A	−2140.9590	1.39
Ni-Tex(MeOH)$_2^+$	C_2	^{3}A	−2141.0101	0.00
Cu-Tex(MeOH)$_2^+$	C_2	^{4}A	−2167.7654	1.16
Cu-Tex(MeOH)$_2^+$	C_2	^{2}A	−2167.8080	0.00
Zn-Tex(MeOH)$_2^+$	C_2	^{3}A	−2037.1671	1.32
Zn-Tex(MeOH)$_2^+$	C_2	^{1}A	−2037.2157	0.00

3.2. Ground-State Geometrical Structures. The geometrical structures of metallotexaphyrins are formally characterized by five possible coordination sites: three pyrrolic- (N_1 and N_2 in Chart 1, structure **1a**) and two imine-nitrogen atoms (N_3 in the same chart). The position of the metal center with respect to the mean plane (ΔN5) formed by the five nitrogen atoms is strongly influenced by the presence, in the crystal structure, of counterions (like Cl$^-$, NO$_3^-$) and/or solvent molecules (MeOH), directly bound to the metal.

Table 2. Selected Bond Lengths (Å) for M(II)-Texaphyrin Complexes[a]

complex	M−N_1	M−N_2	M−N_3	M−O_{MeOH}
Mn-Tex$^+$	2.326 (2.383)	2.179 (2.230)	2.553 (2.539)	/
Mn-Tex(MeOH)$_2^+$	2.348 (2.409)	2.225 (2.236)	2.554 (2.470)	2.265 (2.217)
Fe-Tex$^+$ [b]	2.300	2.137	2.586	/
Fe-Tex(MeOH)$_2^+$ [b]	2.280 (2.321)	2.206 (2.201)	2.580 (2.498)	2.169
Co-Tex$^+$	2.103	2.090	2.815	/
Co-Tex(MeOH)$_2^+$	2.247 (2.335)	2.177 (2.176)	2.635 (2.524)	2.146 (2.116)
Ni-Tex$^+$	2.046	2.073	2.896	/
Ni-Tex(MeOH)$_2^+$	2.119	2.129	2.805	2.111
Cu-Tex$^+$	2.032	2.049	2.923	/
Cu-Tex(MeOH)$_2^+$	2.032	2.057	3.049	2.174
Zn-Tex$^+$	2.165 (2.066)	2.113 (2.127)	2.758 (2.912)	/
Zn-Tex(MeOH)$_2^+$	2.108 (2.139)	2.152 (2.138)	2.866 (2.790)	2.160 (2.137)

[a] In parentheses are reported averaged experimental values obtained from X-ray structures. [b] Experimental data are relative to μ-oxo Fe(III) texaphyrin dimer

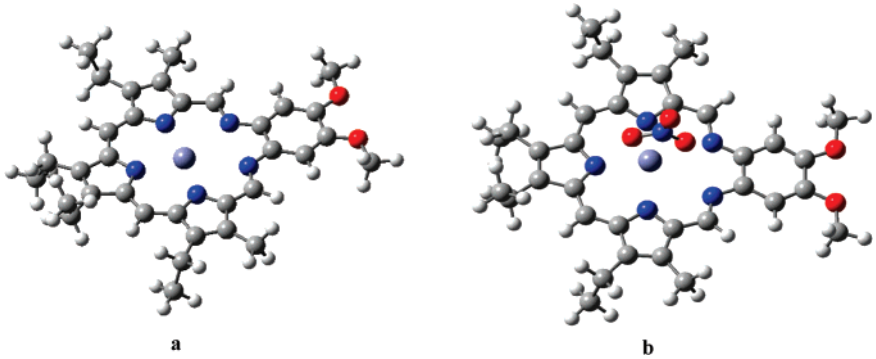

Figure 1. Optimized molecular structures for the Zn-Tex$^+$ bare complex (a) and in the presence of the counterion NO_3^- (b).

Structural data, obtained from single-crystal X-ray analysis are available for all M-Tex$^+$, in organic soluble form, with the exception of Ni- and Cu-Tex$^+$ complexes,[9] so a direct comparison between experimental and computed geometrical data is possible. Selected optimized metal−nitrogen (M−N) and metal−oxygen (M−O) bond lengths are reported in Table 2. Figure 1 shows the resulting optimized structure of Zn-Tex$^+$ and Zn-Tex-NO_3. Owing to the symmetry constraint C_2 axis imposed to the nuclear framework, we can distinguish three kinds of metal−nitrogen bonds (M−N_1, M−N_2, M−N_3); the experimental data, given in parentheses, are referred to as the relative bond lengths averaged around the ideal C_2 axis. For the bare systems, the distance M−N_1 (central pyrrolic nitrogen) ranges from 2.030 to 2.326 Å, decreasing slightly on going from Mn- to Cu-Tex$^+$ and thereafter increases for Zn-Tex$^+$. A similar trend is found for the M−N_2 distance, which changes from 2.049 to 2.225 Å. The metal−imine nitrogen bond length (M−N_3) increases from Fe- to Cu-Tex$^+$, as a geometric consequence of the reduced M−N(pyrrolic) distance. For the Mn-Tex$^+$ complex the difference between the experimental and the computed metal−nitrogen distance is about 0.05 Å for both M−N_1 and M−N_2 and 0.01 Å for M−N_3. The experimental value of the distance of the metal from the N5 mean plane is 0.37 Å. This value is due to the presence of the counterion Cl^-, directly bound to the metal, that allows an out-of-plane movement of the metal, giving rise to an increased M−N_1 and M−N_2 distances. In all calculated structures the metal results are always coplanar with nitrogen atoms, also by relaxing completely the geometry during optimization. Similar considerations are valid for the Zn-Tex$^+$ complex where the presence in the experimental structure of a NO_3^- anion, coordinated to the metal, gives rise to a shift of 0.38 Å for the metal relative to the N5 mean plane. The major discrepancy with experimental data concerns the M−N_3 bond length, whose difference was found to be 0.076 Å; by reoptimizing the structure including the NO_3^- anion, we obtained a good agreement with the experimental counterpart being the difference of 0.01 Å. As a general rule and by excluding the presence of counterions, we found a pentacoordinated geometry for Mn-Tex$^+$ and a tricoordinated one for the other complexes in agreement with experimental findings.[9]

3.3. Gas-Phase Electronic Spectra. The electronic spectra of metallotexaphyrins, like those of metalloporphyrins, are composed of two main absorption bands: one at higher wavelengths, in the visible region, called the Q-band, and the other, at lower wavelengths and more intense, called the B- or Soret band. The electronic spectra of porphyrin-like chromophores were first theoretically rationalized by means of the Gouterman four-orbital model.[45−46] The electronic bands were interpreted in terms of electronic transitions, involving the two highest occupied molecular orbitals (denoted HOMO and HOMO-1) and the two lowest unoccupied orbitals (LUMO and LUMO+1). On the basis of the proposed theoretical model the Q-band is mainly due to two electronic transitions, named Q_x and Q_y. The Q_x transition arises from the HOMO → LUMO (in brief notation 0−0) electronic excitation (around 60% on average) with a contribution from the HOMO-1 → LUMO+1 (1−1 notation)

Table 3. Excitation Energies in eV (in Parentheses in nm), Oscillator Strengths *f*, Configurations, and Experimental Data for M-Tex$^+$ Bare Systems in vacuo and Solution

	vacuum					solution (C-PCM)			
state	ΔE	$\times c4$	λ_{max}	main configuration[a]		ΔE	$\times c4$	λ_{max}	expt[b] ΔE
				FB-Tex					
1 ^{1}B	1.98 (625.1)	0.0661	2.03	70%(0−0) + 28%(1−1)		1.96 (633.4)	0.1083	2.01	1.72
2 ^{1}A	2.07 (598.8)	0.0982	(609.8)	64%(1−0) + 37%(0−1)		2.05 (605.5)	0.1761	(617.3)	(721)
				Mn-Tex$^+$					
1 B	1.92 (646.0)	0.0766	2.00	20%(0−0) + 30%(1−1)	α	1.93 (642.5)	0.1357	2.00	1.71
			(621.1)	19%(0−0) + 31%(1−1)	*β*			(621.1)	(727)
2 A	2.06 (601.9)	0.0826		28%(0−1) + 28%(1−0)	α	2.06 (602.8)	0.1411		
				9%(0−1) + 35%(1−0)	*β*				
				Fe-Tex$^+$					
1 B	1.95 (635.5)	0.0541	2.00	16%(0−0) + 30%(1−1)	α	1.96 (631.6)	0.1188	2.01	1.73
			(621.1)	34%(0−0) + 3%(1−1)	*β*			(617.3)	(717)
2 A	2.05 (605.6)	0.0799		32%(0−1) + 30%(1−0)	α	2.06 (601.7)	0.1298		
				5%(0−1) +32%(1−0)	*β*				
				Co-Tex$^+$					
1 A	1.96 (632.3)	0.0584	2.01	22%(0−0) + 36%(1−1)	α	1.96 (632.7)	0.1292	2.01	1.74
			(617.3)	37%(0−0)	*β*			(617.3)	(713)
2 B	2.05 (604.4)	0.0726		35%(0−1) + 27%(1−0)	α	2.05 (604.1)	0.1473		
				8%(0−1) + 31%(1−0)	*β*				
				Ni-Tex					
1 B	1.97 (628.3)	0.0657	2.03	27%(0−0) + 25%(1−1)	α	1.96 (631.5)	0.1142	2.02	1.76
			609.8	22%(0−1) + 32%(1−2)	*β*			(613.5)	(704)
2 A	2.07 (598.8)	0.0924		15%(1−0) +33%(0−1)	α	2.07 (598.9)	0.1486		
				22%(0−2) +32%(1−1)	*β*				
				Cu-Tex$^+$					
1 B	1.99 (622.2)	0.0593	2.03	27%(0−0) +19%(1−1)	α	1.97 (630.1)	0.1013	2.02	/
			(609.8)	35%(0−1)	*β*			(613.5)	
2 A	2.07 (597.7)	0.0909		15%(0−1) +33%(1−0)	α	2.06 (601.8)	0.1560		
				22%(0−2)+32%(1−1)	*β*				
				Zn-Tex$^+$					
1 ^{1}B	1.95 (636.0)	0.0774	2.01	74%(0−0) + 21%(1−1)		1.96 (633.8)	0.1367	2.01	1.76
2 ^{1}A	2.07 (600.0)	0.0883	(617.3)	65%(1−0) + 37%(0−1)		2.07 (599.2)	0.1400	(617.3)	(704)

[a] By convention, in parentheses the first number, *n*, is referred to as the occupied orbital contribution from HOMO-*n*, and the second, *m*, to the virtual one LUMO+*m*. [b] See Table 4, footnote *a*.

of about 40%, whereas the Q_y transition is composed of the HOMO-1 → LUMO (1−0) and HOMO → LUMO+1 (0−1) electronic excitations. In the following we will refer as 'main configuration' to the orbital composition of each vertical excitation energy. Experimental spectroscopic data in solution are available for Mn(II)-, Fe(II)- in monomer form, Co(II)-, Ni(II)-, and Zn(II)-Tex$^+$ complexes, so a direct comparison with the computed values is possible. For these compounds the absorption wavelengths of maximum intensity relative to the Q-like band fall in the range between 1.71 eV (727 nm) and 1.76 eV (704 nm), decreasing as a function of the identity of the metal center by 23 nm in going from the Mn- to the Zn-Tex$^+$ complex. In order to decouple the effect of the metal and the solvent on the excitations energies, we analyzed first the electronic spectra for bare systems in comparison with the metal-free texaphyrin in monoprotonated form FB-Tex (Chart 1, compound **1a**). Computed vertical excitation energies giving rise to the Q-like band are collected in Table 3 together with the maximum absorption excitation energies obtained from the convolution of the theoretical data by the overlapping of Gaussian functions. From this table we can infer that for each molecule there are only two excitation energies that contribute to the Q-band. For instance, for the closed-shell Zn-Tex$^+$, the first excitation energy is at 1.95 eV ($f = 0.0774$) and arises mainly from HOMO → LUMO (74%) and HOMO-1 → LUMO+1 (21%) electronic excitations. Therefore, on the basis of the Gouterman scheme it can be assigned to the Q_x-type transition. The second excitation energy is at 2.07 eV ($f = 0.0883$), and its main configuration is composed by HOMO-1 → LUMO (65%) and HOMO → LUMO+1 (37%) electronic transitions. This means that this is the Q_y transition. In both cases the transitions have a $\pi \rightarrow \pi^*$ type character, as can be deduced from the plot of the frontier molecular orbitals in Figure 2. Similar results are obtained for the free-metal form of texaphyrin, which presents the first excitation energy at 1.98 eV (Q_x-transition) and the second one at 2.07 eV (Q_y-transition). On the other hand, to describe the transitions for the open shell systems, we have to consider the α- and *β*-electron excitations. For instance, for the Fe-Tex$^+$ complex we found the first excitation energy at 1.95 eV ($f = 0.041$), whose main configuration is

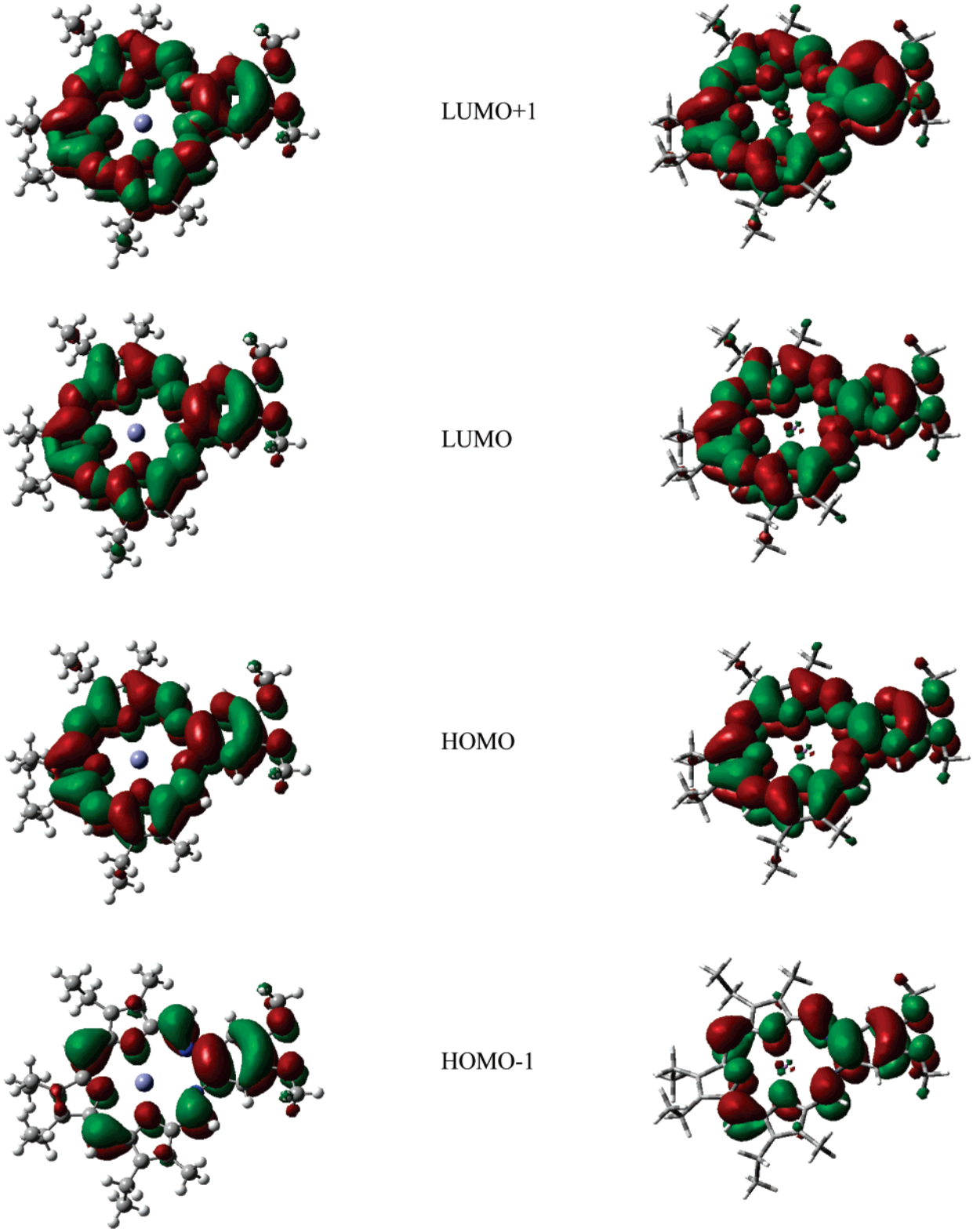

Figure 2. Molecular orbital plot of the four 'Gouterman orbitals' for Zn-Tex$^+$ (on the left) and Mn-Tex$^+$ (alpha orbitals).

composed of the alpha HOMO → LUMO and HOMO −1 → LUMO+1 electronic transitions, contributing respectively for 16% and 30%, and the beta HOMO → LUMO transition for 34%. The second excitation energy is at 2.05 eV ($f =$ 0.0799) and is composed of HOMO-1 → LUMO and HOMO → LUMO+1 for both alpha and beta electronic transitions. For the other complexes the previously described Gouterman scheme is obeyed with some exceptions that, in any case, do not introduce significant changes. Since the experimental data are relative to the maximum absorption wavelengths λ_{max} for the Q- and B-band, it seems more appropriate to compare these data with those obtained from the simulation of the spectra and in particular with the computed maximum absorption wavelengths for the Q-band (Table 3). As can be inferred, all values relative to E_{max} for the Q-band are overestimated in energy with respect to the experimental

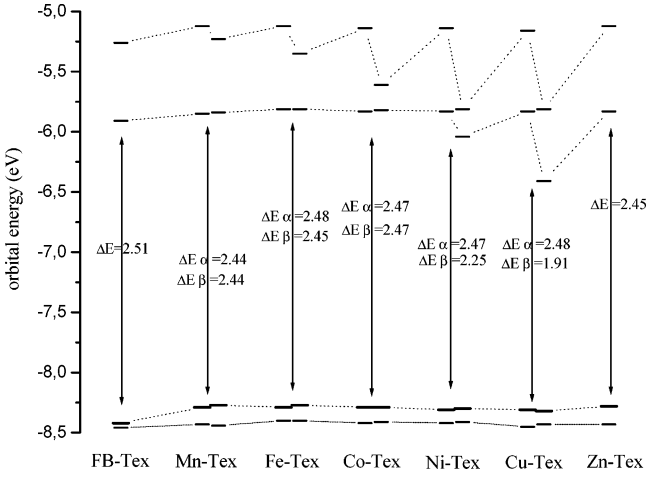

Figure 3. Energy molecular diagram for the four 'Gouterman orbitals' of M-Tex$^+$.

ones, and the difference ranges from 0.25 eV for Zn-Tex$^+$ to 0.29 eV for Mn-Tex$^+$. As found in previous works based on the same level of theory (PBE0/6-31G*//PBE0/6-31+G*), the theoretical error is not larger than 0.3 eV for transition metals containing systems. The influence of the metal on the Q-band relative to the free-metal texaphyrin is in general slight, with the maximum difference of 11 nm for Mn-Tex$^+$ and Fe-Tex$^+$. As mentioned above, for the experimental spectra the maximum absorption wavelength λ_{max} for the Q-band is blue-shifted in going from the Mn- to the Zn-Tex$^+$ complex. In our case this trend is qualitatively followed except for the zinc complex. It is also worth noting that for Cu-Tex$^+$ there are no spectroscopic data since the compound was not well characterized by diffraction analysis. Therefore, we cannot decide whether the breakdown of this trend, at the theoretical level, occurs for the Cu-Tex$^+$ or the Zn-Tex$^+$ complex. Some hints for the theoretical analysis could come also from the orbital energy diagram in Figure 3, which reports the energetic behavior of the four Gouterman orbitals across the series of the complexes. The first point to note is the regular aspect of the diagram for the energetic gap HOMO−LUMO, which does not show drastic changes along the series. As a consequence, the influence of the metal is confirmed to be small on the excitation energies. An exception could be represented by the β-gap for Cu-Tex$^+$ that, however, does not contribute to the transition (see Table 2). The free-metal texaphyrin has the highest gap (2.51 eV), whereas for the unique closed shell Zn-Tex$^+$ system a value of 2.45 eV is calculated corresponding to an increased excitation energy E_{max}. The Zn-Tex$^+$ complex has no metal contribution to the frontier orbitals, as deduced from the molecular orbitals plot in Figure 2. For the other systems we have to consider the α and β energetic levels: while the α HOMO−LUMO gap changes little going from Mn- to Cu-Tex$^+$ (0.04 eV), the β gap decreases by about 0.5 eV.

4. Solvent Effects

The basic interest in metallotexaphyrins lies in their use as photosensitizers in photodynamic therapy (PDT), so they should be thermodynamically stable in a biological environment in which water is the main component and preserve their spectroscopic features in this medium. A theoretical analysis accounting for solvent effects on the spectroscopic properties of the photosensitizer can give more insights for a better description of the overall mechanism. The class of metallotexaphyrins under study is soluble in methanol solvent, though water-soluble analogues have been synthesized for Mn(II), Co(II), and Fe(III). The iron complex was characterized by diffraction analysis as a μ-oxo dimer. The water-soluble metal complexes bear an alcohol ($R_1 = -CH_2-CH_2OH$) and a polyethylene glycol [$R_2 = CH_2CH_2O)_3CH_3$] as side-chain substituents that increase their hydrophilic properties. The experimental maximum absorption wavelength in the Q-band region for the water-soluble Mn(II)-Tex$^+$ falls at 730 nm, and the wavelength difference with the methanol-soluble form amounts only to 3 nm. For that reason we can argue that the influence of the solubilizing substituents is negligible on the Q-band spectral properties. Therefore, the methanol-soluble complexes can represent an appropriate theoretical model for the study of solvent effects also for biological media. The influence of methanol molecules can be considered implicitly by using a continuum solvent model or explicitly by adding a few solvent molecules to the complex. The latter approach seems reasonable since the metal center tends to complete its coordination sphere as also experimentally found. At the same time, the reaction field generated by the interaction with the bulk solvent could change the electronic distribution and therefore the photochemical properties. In recent works, the coupling of continuum solvent models with explicit treatment of solvent molecules was used to well reproduced UV−vis electronic spectra. As a first step we applied the conductor-like polarizable continuum model (C-PCM) to the optimized M(II)-Tex$^+$ structures, as single-point TD-DFT calculations, without adding solvent molecules. From the results reported in Table 3, it is worth noting that the excitation energies are only slightly affected by the reaction field for almost all of the compounds, the difference being within 0.01 eV in the absolute value for the M-Tex$^+$'s. The oscillator strength for every excitation energy results to be increased for all the compounds with respect to the vacuum state. Regarding the maximum absorption wavelengths λ_{max}, the FB-Tex, Ni-Tex$^+$, and Cu-Tex$^+$ are red-shifted, improving the accordance with the experimental data, whereas for the other complexes the λ_{max} result is unchanged.

4.1. Supramolecular Model. In the supramolecular approach two methanol molecules were added, directly bound to the metal center, as suggested from the crystallographic structures of Mn-, Co-, and Zn-Tex$^+$, and the structures were fully optimized in C_2 symmetry. The determination of the most stable electronic state and the gap between the ground and first excited state was discussed previously in section 3.1. The distances between the metal and the oxygen atoms, as listed in Table 2 (M−O), show a good agreement with the experimental bond lengths, with a difference within 0.048 Å. For these structures we reported in Table 4 the vertical excitation energies, the oscillator strengths, and the main configuration computed in vacuo and including also the bulk solvent effects (C-PCM). In both cases the behavior follows again the four-orbitals Gouterman's model. For Mn-, Co-,

Table 4. Excitation Energies in eV (in Parentheses in nm), Oscillator Strengths *f*, Configurations, and Experimental Data for M-Tex$^+$ Complexes with Two Methanol Molecules, in vacuo and Solution

vacuum				solution (methanol C-PCM)				
state	ΔE	$\times c4$	main configuration[a]		ΔE	$\times c4$	main configuration[a]	expt[b] ΔE
				Mn-Tex$^+$				
1 B	1.97 (630.9)	0.0780	28%(0−0) + 29%(1−1) 38%(0−0)	α β	1.96 (633.0)	0.1207	27%(0−0) + 28%(1−1) 40%(0−0)	1.71 (727)
2 A	2.11 (586.8)	0.0575	29%(1−0) + 23%(0−1) 35%(1−0) + 12%(0−1)	α β	2.09 (592.5)	0.1105	23%(0−1) + 32%(1−0) 37%(1−0) + 8%(0−1)	
				Fe-Tex$^+$				
1 B	1.97 (629.1)	0.0502	29%(0−0) + 5%(1−1) + 6%(3−0) 6%(0−0) + 8%(1−0) + 5%(2−1) + 6%(5−0)	α β	1.96 (630.7)	0.0953	34%(0−0) + 3%(1−1) + 5%(3−0) 5%(0−0) + 14%(1−0) + 38% (2−1)	1.73 (717)
2 B	2.01 (616.3)	0.0372	7%(0−0) + 57%(1−1) 8%(0−0) + 21%(1−0) + 10%(2−1)	α β	2.00 (618.8)	0.0444	4%(0−0) + 58%(1−1) 4%(0−0) +21%(1−0) + 16%(2−1)	
3 A	2.13 (582.6)	0.0648	32%(1−0) + 14%(0−1) 4%(1−1) + 18%(0−1) + 32%(2−0)	α β	2.11 (588.6)	0.1219	35%(1−0) +10%(0−1) 13%(0−1) + 8%(1−1) + 35%(2−0)	
				Co-Tex$^+$				
1 B	1.99 (621.9)	0.0812	37%(0−0) +8%(1−1) 37%(0−0) + 13%(1−1)	α β	1.97 (628.4)	0.1312	40%(0−0) + 2%(1−1) 34%(0−0) + 18%(1−1)	1.74 (713)
2 A	2.09 (592.6)	0.0848	34%(1−0) +13%(0−1) 33%(1−0) +21%(0−1)	α β	2.09 (592.4)	0.1260	36%(1−0) + 11%(0−1) 35%(1−0) + 19%(0−1)	
				Ni-Tex$^+$				
1 B	2.02 (615.0)	0.0822	35%(0−0) + 12%(1−1) 39%(0−0) + 9%(1−1)	α β	2.00 (621.5)	0.1327	36%(0−0) + 11%(1−1) 41%(0−0) + 7%(1−1)	1.76 (704)
2 A	2.10 (589.6)	0.0708	34%(1−0) + 13%(0−1) 32%(1−0) +22%(0−1)	α β	2.10 (590.7)	0.1178	36%(0−1) + 11%(0−1) 34%(0−1) + 20%(0−1)	
				Cu-Tex$^+$				
1 B	1.96 (633.2)	0.0726	19%(0−0) +28%(1−1) 21%(0−0) + 28%(1−2)	α β	1.94 (638.6)	0.1068	39%(0−0) + 3%(1−1) 36%(0−0) + 15%(1−1)	/
2 A	2.10 (589.5)	0.0745	34%(1−0) + 13%(0−1) 31%(1−0) + 22%(0−1)	α β	2.07 (597.6)	0.1450	37%(1−0) +9%(0−1) 33%(1−0) + 21%(0−1)	
				Zn-Tex$^+$				
1 ^{1}B	1.97 (629.6)	0.0849	74%(0−0) + 21%(1−1)		1.96 (632.9)	0.1304	77%(0−0) + 18%(1−1)	1.76 (704)
2 ^{1}A	2.11 (587.2)	0.0582	65%(1−0) + 36%(0−1)		2.09 (594.4)	0.1176	70%(1−0) + 31%(0−1)	

[a] By convention, in parentheses the first number, *n*, is referred to as the occupied orbital contribution from HOMO-*n*, and the second, *m*, to the virtual ones LUMO+*m*. [b] See Table 3, footnote *a*.

Ni-, and Zn-Tex$^+$, in vacuo, only two excitations energies contribute to the Q-band. On the basis of the main configuration for these compounds we can assign these two excitations to a Q_x-type transition for the lowest excitation energy and to a Q_y-type transition for the next excitation energy, according to what was outlined for the electronic spectra of M-Tex$^+$ bare systems (section 3.2). For the Fe-Tex$^+$ complex, we found a different behavior regarding the number of excitation energies and their main configuration. Indeed, we found three excitation energies contributing to the Q-like band, with the main configuration that includes also orbital contributions to the electronic transitions other than the four Gouterman's orbitals. The introduction of the bulk solvent effects, through the C-PCM method, in the case of complexes coordinating to solvent molecules results in a slight decrease of the excitation energies (maximum deviation of 0.03 eV for Cu-Tex$^+$) and an increase of the relative oscillator strengths. An overall picture of the simulated electronic spectra of Zn-Tex$^+$, with and without explicit solvent molecules, and of the theoretical trend for the maximum intensity excitation energies (in eV) of all the compounds are given in Figures 4 and 5, respectively. In the latter case the mean deviation from the experimental data is found to be +0.3 eV, both for the vacuum and implicit solvation models.

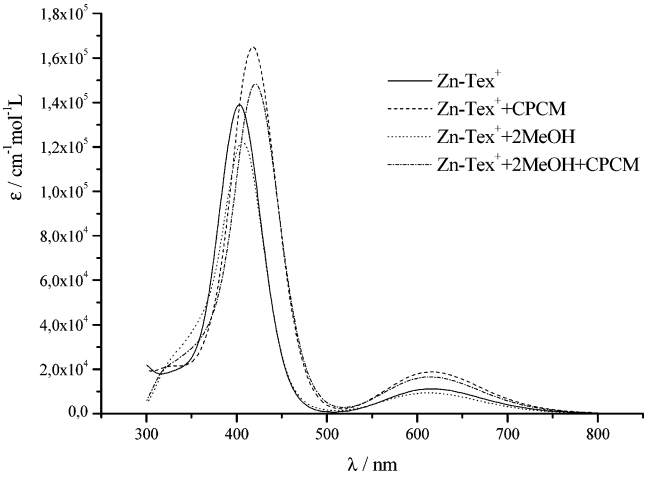

Figure 4. Simulated electronic spectra for the Zn-Tex$^+$ complex both in the gas phase and methanol solution (C-PCM), with and without explicit solvent molecules.

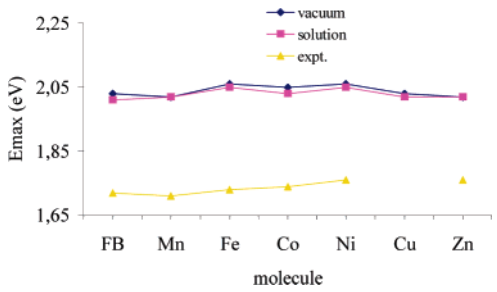

Figure 5. Theoretical and experimental trend of λ_{max} in the Q-band region for M-Tex$^+$ with two methanol molecules, in vacuo and in solution.

As suggested by one of the referees of this work we verified whether the scalar relativistic contributions can account for this error using relativistic pseudopotentials (see Computational Details section) for test calculations on the Zn-Tex$^+$ complex. The results clearly show that no significant change for the excitation energies occurs with respect to the chosen pseudopotential (LANL2DZ). In fact, using both relativistic ECP's[31,32] with 10 and 28 core electrons excitation energies of the Q-band are at 1.95 eV (Q_x) and 2.07 eV (Q_y).

5. Conclusions and Remarks

In the present work we studied the ground-state geometries and electronic absorption spectra of late first-row metal texaphyrin at the density functional level of theory both in vacuo and in methanol solution. Ground-state properties like geometrical parameters and vertical electronic excitations, were computed, analyzed, and compared with available experimental data. Owing to the use of these compounds in photodynamic therapy, particular attention was devoted to two spectral aspects, important for the design of an ideal photosensitizer: (a) determination of the energetic gap between ground and first excited states and (b) computation of the Q-band maximum absorption wavelengths and corresponding molecular orbital contribution to the electronic transitions. The influence of the solvent on the excitation energies was investigated by using polarizable dielectric continuum model (C-PCM) and including explicit solvent molecules as axial ligands to the metal center. In both cases the excitation energies are overestimated by about 0.3 eV in comparison with experimental data. About the energetic behavior, all compounds with two solvent molecules, except Co-Tex$^+$, have an energetic gap between the ground and the first excited state greater than 0.98 eV and fulfill one of the requirements for their application as a photosensitizer in PDT. Hopefully this theoretical investigation of the electronic and spectroscopic properties of a class of metallotexaphyrins could give some hints for the design of more efficient agents in photodynamic therapy.

Acknowledgment. Financial support from the Università degli Studi della Calabria and Regione Calabria (POR Calabria 2000/2006, misura 3.16, progetto PROSICA) is gratefully acknowledged.

References

(1) Sessler, J. L.; Murai, T.; Lynch, V.; Cyr, M. *J. Am. Chem. Soc.* **1988**, *110*, 5586−5588.

(2) Sessler, J. L.; Hemmi, G.; Mody, T. D.; Murai, T.; Burrell, A.; Young, S. W. *Acc. Chem. Res.* **1994**, *27*, 43−50.

(3) Sessler, J. L. et al. *Coord. Chem. Rev.* **2003**, *240*, 17−55.

(4) Sessler, J. L.; Mody, T. D.; Hemmi, G.; Lynch, V. *Inorg. Chem.* **1993**, *32*, 3157−3187.

(5) Guldi, D. M.; Mody, T. D.; Gerasimchuk, N.; Magda, D.; Sessler, J. L. *J. Am. Chem. Soc.* **2000**, *122*, 8289−8298.

(6) Maiya, B. G.; Harrman, A.; Sessler, J. L.; Hemmi, G.; Murai, T.; Mallouk, T. E. *J. Phys. Chem.* **1989**, *93*, 8111−8115.

(7) Sessler, J. L.; Tvermoes, N. A.; Guldi, D. M.; Mody, T. D.; Allen, W. E. *J. Phys. Chem. A* **1999**, *103*, 787−794.

(8) Shimanovich, R.; Hannah, S.; Lynch, V.; Gerasimchuk, N.; Mody, T. D.; Magda, D.; Sessler, J. L.; Groves, J. T. *J. Am. Chem. Soc.* **2001**, *123*, 3613−3614.

(9) Hannah, S.; Lynch, V.; Guldi, D. M.; Gerasimchuk, N.; MacDonald, C. L. B.; Magda, D.; Sessler, J. L. *J. Am. Chem. Soc.* **2002**, *124*, 8416−8427.

(10) Hannah, S.; Lynch, V.; Gerasimchuk, N.; Magda, D.; Sessler, J. L. *Org. Lett.* **2001**, *3*, No. 24, 3911−3914.

(11) Rosenthal, D. I.; Nurenberg, P.; Becerra, C. R.; Frenkel, E. P.; Carbone, D. P.; Lum, B. L.; Miller, R.; Engel, J.; Young, S.; Miles, D.; Renschhler, M. F. *Clin. Cancer Res.* **1999**, *5*, 739−745.

(12) Viala, J.; Vanel, D.; Meingan, P.; Lartigau, E.; Carde, P. *Radiology* **1999**, *212*, 755−759.

(13) MacDonald, I. J.; Dougherty, T. J. *J. Porphyrins Phthalocyanines* **2001**, *5*, 105−129.

(14) Van Tenten, Y.; Schuitmaker, H. J.; De Wolf, A.; Willekens, B.; Vrensen, G. F. J. M.; Tassignon, M. J. *Exp. Eye Res.* **2001**, *72*, 41−48.

(15) Dolmans, D. E. J. G. J.; Fukumura, D.; Jain, R. K. *Nat. Rev. Cancer* **2003**, *3*, 380−387.

(16) DeRosa, M. C.; Crutchley, R. J. *Coord. Chem. Rev.* **2002**, *233−234*, 351−371.

(17) Schweitzer, C.; Schimidt, R. *Chem. Rev.* **2003**, *103*, 1685−1757.

(18) Cao, X.; Dolg, M. *Mol. Phys.* **2003**, *101*, 2427−2435.

(19) Cao, X.; Li, Q.; Moritz, A.; Xie, Z.; Dolg, M.; Chen, X.; Fang, W. *Inorg. Chem.* **2006**, *45*, 3444−3451.

(20) Waluk, J.; Michl, *J. Org. Chem.* **1991**, *56*, 2729−2735.

(21) Casida, M. E.; Time-Dependent Density Functional Response Theory for Molecules. In *Recent Advances in Density Functional Methods*, 1st ed.; Chong, D. P., Ed.; Word Scientific: Singapore, Singapore, 1995; Vol. 1, pp 155−192.

(22) Frisch, M. J.; Trucks, G. W.; Schlegel, H. B.; Scuseria, G. E.; Robb, M. A.; Cheeseman, J. R.; Montgomery, J. A., Jr.; Vreven, T.; Kudin, K. N.; Burant, J. C.; Millam, J. M.; Scalmani, G.; Rega, N.; Petersson, G. A.; Nakatsuji, H.; Hada, M.; Ehara, M.; Toyota, K.; Fukuda, R.; Hasegawa, J.; Ishida, M.; Nakajima, T.; Honda, Y.; Kitao, O.; Nakai, H.; Klene, M.; Li, X.; Knox, J. E.; Hratchian, H. P.; Cross, J. B.; Bakken, V.; Adamo, C.; Jaramillo, J.; Gomperts, R.; Stratmann, R. E.; Yazyev, O.; Austin, A. J.; Cammi, R.; Pomelli, C.; Ochtersky, J. W.; Ayala, P. Y.; Morokuma, K.;

Voth, G. A.; Salvador, P.; Dannenberg, J. J.; Zakrzewski, V. G.; Dapprich, S.; Daniels, A. D.; Strain, M. C.; Farkas, O.; Malick, D. K.; Rabuck, A. D.; Raghavachari, K.; Foresman, J. B.; Ortiz, J. V.; Cui, Q.; Baboul, A. G.; Clifford, S.; Cioslowski, J.; Stefanov, B. B.; Liu, G.; Liashenko, A.; Piskorz, P.; Komaromi, I.; Martin, R. L.; Fox, D. J.; Keith, T.; Al-Laham, M. A.; Peng, C. Y.; Nanayakkara, A.; Challacombe, M.; Gill, P. M. W.; Johnson, B.; Chen, W.; Wong, M. W.; Gonzalez, C.; Pople, J. A. *Gaussian03, revision B.05*; Gaussian, Inc.: Wallingford, CT, 2004.

(23) Ernzerhof, M.; Scuseria, G. E. *J. Chem. Phys.* **1999**, *110*, 5029−5036.

(24) Adamo, C.; Barone, J. *J. Chem. Phys.* **1999**, *110*, 6158−6170.

(25) Perdew, J. P.; Burke, K.; Ernzerhof, M. *Phys. Rev. Lett.* **1996**, *77*, 3865−3868.

(26) Hariharan, P. C.; Pople, J. A. *Theor. Chim. Acta* **1973**, *28*, 213.

(27) Gill, P. M. W.; Johnson, B. G.; Pople, J. A.; Frisch, M. J. *Chem. Phys. Lett.* **1992**, *197*, 499.

(28) Hay, P. J.; Wadt, W. R. *J. Chem. Phys.* **1995**, *82*, 270−283.

(29) Francl, M. M.; Petro, W. J.; Hehre, W. J.; Binkley, J. S.; Gordon, M. H.; DeFree, D. J.; Pople, J. A. *J. Chem. Phys.* **1982**, *77*, 3654−3665.

(30) Stratmann, R. E.; Scuseria, G. E.; Frisch, M. J. *J. Chem. Phys.* **1998**, *109*, 8218−8224.

(31) Dolg, M.; Wedig, U.; Stoll, H.; Preuss, H. *J. Chem. Phys.* **1987**, *86*, 866−872.

(32) Schautz, F.; Flad, H. J.; Dolg, M. *Theor. Chem. Acc.* **1998**, *99*, 231−240.

(33) Petit, L.; Quartarolo, A. D.; Adamo, C.; Russo, N. *J. Phys. Chem. B* **2006**, *110*, 2398−2404.

(34) Quartarolo, A. D.; Russo, N.; Sicilia, E. *Chem. Eur. J.* **2006**, *12*, 16797−16803.

(35) Petit, L.; Adamo, C.; Russo, N. *J. Phys. Chem. B* **2005**, *109*, 12214−12221.

(36) Petit, L.; Maldivi, P.; Adamo, C. *J. Chem. Theory Comput.* **2005**, *1*, 953−962.

(37) Tomasi, J.; Persico, M. *Chem. Rev.* **1994**, *94*, 2027−2094.

(38) Tomasi, J.; Mennucci, B.; Cammi, R. *Chem. Rev.* **2005**, *105*, 2999−3093.

(39) Barone, V.; Cossi, M. *J. Phys. Chem. A* **1998**, *102*, 1995−2001.

(40) Cossi, M.; Barone, V. *J. Chem. Phys.* **2001**, *115*, 4708−4717.

(41) Scalmani, G.; Frisch, M. J.; Mennuci, B.; Tomasi, J.; Cammi, R.; Barone, V. *J. Chem. Phys.* **2005**, *124*, 94107−94121.

(42) Santoro, F.; Barone, V.; Gustavsson, T.; Improta, R. *J. Am. Chem. Soc.* **2006**, *128*, 16312−16322.

(43) Improta, R.; Barone, V.; Santoro, F. *Angew. Chem., Int. Ed.* **2007**, *46*, 405−408.

(44) Gorelsky, S. I. *SWizard program*; York University: Toronto, Canada, 1998. http: //www.sg-chem.net/ (accessed Sep 2006).

(45) Gouterman, M. *J. Mol. Spectrosc.* **1961**, *6*, 138−163.

(46) Gouterman, M.; Wagniere, G. H.; Snyder, L. C. *J. Mol. Spectrosc.* **1963**, *11*, 108−127.

CT600376H